

First-Principles Study of Hydrogen Dynamics in Monoclinic TiO

S. Vahid Hosseini,^{1,2} Andrei Postnikov,² and Mohammad Reza Mohammadzadeh¹

¹*Superconductivity Research Laboratory (SRL), Department of Physics,*

University of Tehran, North Kargar Ave., P. O. Box 14395-547, Tehran, Iran

²*LCP-A2MC, Université de Lorraine, 1 Bd Arago, F-57078 Metz Cedex 3, France*

The existence of intrinsic vacancies in cubic (monoclinic) TiO suggests opportunity for hydrogen absorption, which was addressed in recent experiments. In the present work, based on first principles calculations, the preferences are studied for the hydrogen absorption sites and diffusion paths between them. The oxygen vacancies are found to be the primary hydrogen traps with absorption energy of -2.87 eV. The plausible channels for hydrogen diffusion between adjacent vacancy sites (ordered in the monoclinic TiO structure) are compared with the help of calculations using the nudged elastic band method. Several competitive channels are identified, with barrier heights varying from 2.87 to 3.71 eV, that is high enough to ensure relative stability of trapped hydrogen atoms at oxygen vacancy sites. Moreover, the possibility of adsorption of molecular hydrogen was tested and found improbable, in the sense that the H_2 molecules penetrating the TiO crystal are easily dissociated (and released atoms tend to proceed towards oxygen vacancy sites). These results suggest that hydrogen may persist in oxygen vacancy sites up to high enough temperatures.

I. INTRODUCTION

The present work aims at elucidating hydrogen trapping and mobility in titanium monoxide. This subject falls within a relatively small intersection of vast domains of research. The hydrogen absorption, storage and processing in materials is a tremendous and rapidly evolving field; a recent review by Abe *et al.* [1] may serve a nice introduction into the subject. Transition metal oxides are omnipresent in materials science through their different manifestations, over which a concise review by Goodeenough [2] offers an efficient guideline. In what regards specifically the hydrogen problematics, transition metal oxides typically appear as elements of surface protection of metals or as catalytic agents, e.g., in a promising research field of water splitting on oxide-based electrocatalysis [3], explained, e.g., in recent reviews by Zhu *et al.* [4], Song *et al.* [5] and Shang *et al.* [6]. Burke *et al.* [7] summarized the trends in the activity of different transition metal oxides as catalysts for the *oxygen evolution reaction*. The phenomenon of *hydrogen spillover* came into discussion, in which molecular hydrogen dissociates at the metal surface, and protons diffuse into the catalytic oxide support – see, e.g., Ref. 8 concerning the process on MgO, or Ref. 9 for the reaction on VO₂. Whittingham [10] described hydrogen motion in metal oxides; Nolan and Browne [11] overviewed chemical reactions relevant in oxides in relation with hydrogen energy problematics.

Still narrowing the subject, the works from this category dealing with titanium are not numerous, and predominantly concern the dioxide. Oelerich *et al.* [12, 13] studied catalytic activity of *3d* metal oxides, including TiO₂, and concluded that a tiny addition of them noticeably enhanced hydrogen sorption kinetics of nanocrystalline magnesium. Yin *et al.* [14] studied, in experiment supported by first-principles calculations, the adsorption of hydrogen on the surface of TiO₂ with possible diffusion into the depth. Feng *et al.* [15] looked into effect of oxygen vacancies in TiO₂ on the enhancing of electro-

catalytic activity for *hydrogen evolution reaction* (HER). Oxygen vacancies also play an important role in shaping the *oxygen evolution reaction* essential for water splitting. A recent review on these issues by Zhu *et al.* [16] covers, among a long list of oxides studied, works on titanium dioxide and oxide-nitride. Hu *et al.* [17] praised micro- and mesoporous Ti oxides as “in many ways ideal candidates for hydrogen storage because they can be made from inexpensive and light metal Ti, and the surface area, pore size, and wall thickness can be systematically controlled”. Li *et al.* [18] studied the hydrogen evolution activity in epitaxially grown Ti₂O₃ polymorphs.

Titanium monoxide enters the picture as Swaminathan *et al.* [19] reported that strongly reduced titania (with nominal composition TiO_{1.23}, the crystal structure of which reveals X-ray diffraction peaks of disordered TiO) exhibits enhanced HER activity. Recently, Skripov *et al.* [20] investigated hydrogen absorption in substoichiometric TiO (TiO_{0.72}H_{0.30} and TiO_{0.96}H_{0.14}) by a combined use of X-ray and neutron diffraction, neutron vibrational spectroscopy and nuclear magnetic resonance. This work led to the following conclusions: (*i*) in both nearly stoichiometric and strongly substoichiometric (oxygen-deficient) samples, hydrogen atoms resided exclusively at O vacancy sites; (*ii*) the hydrogenation of nearly stoichiometric, originally B1 disordered, phase provokes an emergence of an ordered (Ti₅O₅ monoclinic) phase coexisting with the disordered (B1-structure) TiO; (*iii*) hydrogen diffusion seems to be insignificant; (*iv*) vibrations of hydrogen atoms occur throughout a broad range of frequencies, presumably as a manifestation of different environments (a possible symmetry-lowering off-center displacement of the trapped hydrogen; a completeness or not of its coordinating Ti octahedron) occurring at different O vacancy sites.

TiO can be crystallized in cubic B1 (NaCl-type) structure, allowing broad limits of deviation from stoichiometry in the nominal formula TiO_{*x*}, namely (citing Watanabe *et al.* [21]) $0.9 \leq x \leq 1.25$ at 990°C and $0.7 \leq x \leq 1.25$

at 1400°C. As mentioned further in Ref. 21, even in equiatomic compound about 15% of both titanium and oxygen sites are vacant. The vacancies are randomly distributed at high temperatures, however on rapid cooling from 1400 to 990 °C, they get ordered, resulting in a monoclinic phase, which is in fact the underlying B1 with 1/6 of sites on each sublattice being vacant. While deficiency on either cation or anion sublattice is not uncommon in materials, the coexistence of vacancies in both sublattices is relatively rare and, among the metal monoxides, is known to occur only in TiO [22, 23], VO [24] and NbO [25].

Theoretical studies of TiO have a long history. Neckel *et al.* [26] performed self-consistent electronic structure calculation of TiO (among other transition metal oxides and nitrides with B1 structure, assumed perfect and complete). This revealed the essential in the placement and composition of different energy bands. Leung *et al.* [27] compared the relative stability under pressure of several Ti- and O-deficient (stoichiometric) ordered phases, including the “true” monoclinic Ti_5O_5 and several more symmetric ordered-vacancies phases; the energy preference of the monoclinic phase has been demonstrated. Andersson *et al.* [28] offered a more detailed analysis of different vacancy-ordered phases, in comparison with a model of disordered alloy (of vacancies) on each sublattice. (One can add in this relation that a much earlier attempt of a “vacancy-alloying” approach to electronic structure of TiO, non self-consistent and within virtual crystal approximation, was undertaken by Schoen and Denker[29]). Graciani *et al.* [30] in an almost simultaneous work reiterated the established reasons for the structural preference of the monoclinic phase. Kostenko *et al.* [31] concentrated on comparing the ordered monoclinic Ti_5O_5 phase against the B1 vacancy-disordered one, whereby the latter was simulated by averaging the results over 20 different supercells of $(40 \times \text{Ti} + 40 \times \text{O})$ atoms (plus $8 \times \text{Ti} + 8 \times \text{O}$ vacancy sites). Under this perspective, we considered the monoclinic TiO phase to be a perfect model system – not too simplistic yet well defined – for studying hydrogen trapping, vibration, and diffusion. A different choice, that of disordered B1 lattice, would make the results too much dependent on the particular model(s) of disorder used. An ambition of the present work is to challenge the conclusions formulated by Skripov *et al.* [20], on the basis of first-principles calculations, and/or to give these qualitative conclusions a numerical expression. Specifically, we probe adsorption energies of hydrogen at different sites, calculate vibration modes of the crystal doped with hydrogen, identify plausible diffusion paths and estimate corresponding energy barriers.

In its concept, our work has certain similarities with *ab initio* simulation by Kajita *et al.* [32] done for hydrogen adsorption at the TiO_2 surface, in the sense that different trapping sites have been identified, and the energy barriers between them explored. The difference is in the crystal structure of the underlying oxide and in that we

considered 3-dimensional crystal in our simulation, and not a surface represented by a slab.

The present work is organized as follows. Section II explains the crystal structure, adsorption sites and the paths between them. Section III outlines technical details of first-principles calculations. Section IV presents the results of hydrogen binding energy and intersite barriers, with its impact on diffusion. The conclusions are summarized in section V.

II. CRYSTAL STRUCTURE AND GEOMETRY OF VACANCIES

The stable monoclinic structure of nominally stoichiometric TiO (which holds however in the concentration range $\text{TiO}_{0.7}$ through $\text{TiO}_{1.25}$) has been identified by Watanabe *et al.* [21, 33]. In terms of the lattice parameter of the nominal underlying cubic (B1) lattice, and in the setting to be used in the following, the monoclinic lattice comes about spanned by $\mathbf{a} = [201]$, $\mathbf{b} = [010]$, and $\mathbf{c} = [\bar{1}01]$ vectors. Correspondingly, the unit cell contains $3 \times 4 = 12$ of both anionic and cationic sites, of which only 10 (of each species) are occupied. Further on, $a/b = \sqrt{5}$, $c/b = \sqrt{2}$, and $\beta = \pi - \arctan(3) = 108^\circ 26'$. These relations, as we will see, are slightly modified due to the presence of vacancies. The distribution of vacancies centers the (a, b) face (space group $C2/m$, unique axis b), hence the primitive cell in fact includes five Ti and five O atoms. Their arrangement over Wyckoff positions with coordinates refined in experiment can be found in Ref. 21. The unit cell, in several side views (with different diffusion paths, see below) and as a $[010]$ projection of two consecutive atomic planes $y = 0$ and $y = \frac{1}{2}$, is shown in Fig. 1. The choice of the unit cell is such that Ti vacancy is at the origin. These projection figures specify, for further reference, the numbering of Ti_4O_4 cuboids (eventually with vacancies, represented by squares instead of circles, at some vertices) centered in the $y = \frac{1}{4}$ and $y = \frac{3}{4}$ planes.

A priori, the possible hydrogen absorption sites are expected to possess certain symmetry; plausible candidates are interstitial positions (inside the Ti_4O_4 cuboids, probably with one or two corner atoms missing), the Ti vacancy sites, or the O vacancy sites. All these possibilities have been explored (see the details below), with the conclusion that the oxygen vacancies are the ground-state configurations, Ti vacancies are metastable local minima, and the other trial configurations end up squeezed out into one or the other of the two mentioned. Anticipating the question of hydrogen diffusion between the oxygen vacancy sites, we can already elaborate on the possible trajectories connecting such adjacent positions. Fig. 1 summarizes all possible paths connecting adjacent O vacancies, shown as straight-line fragments through the centers of different (numbered) cuboids. In practical calculations using the Nudged Elastic Band (NEB, see below) technique, the trajectories will be shortened /

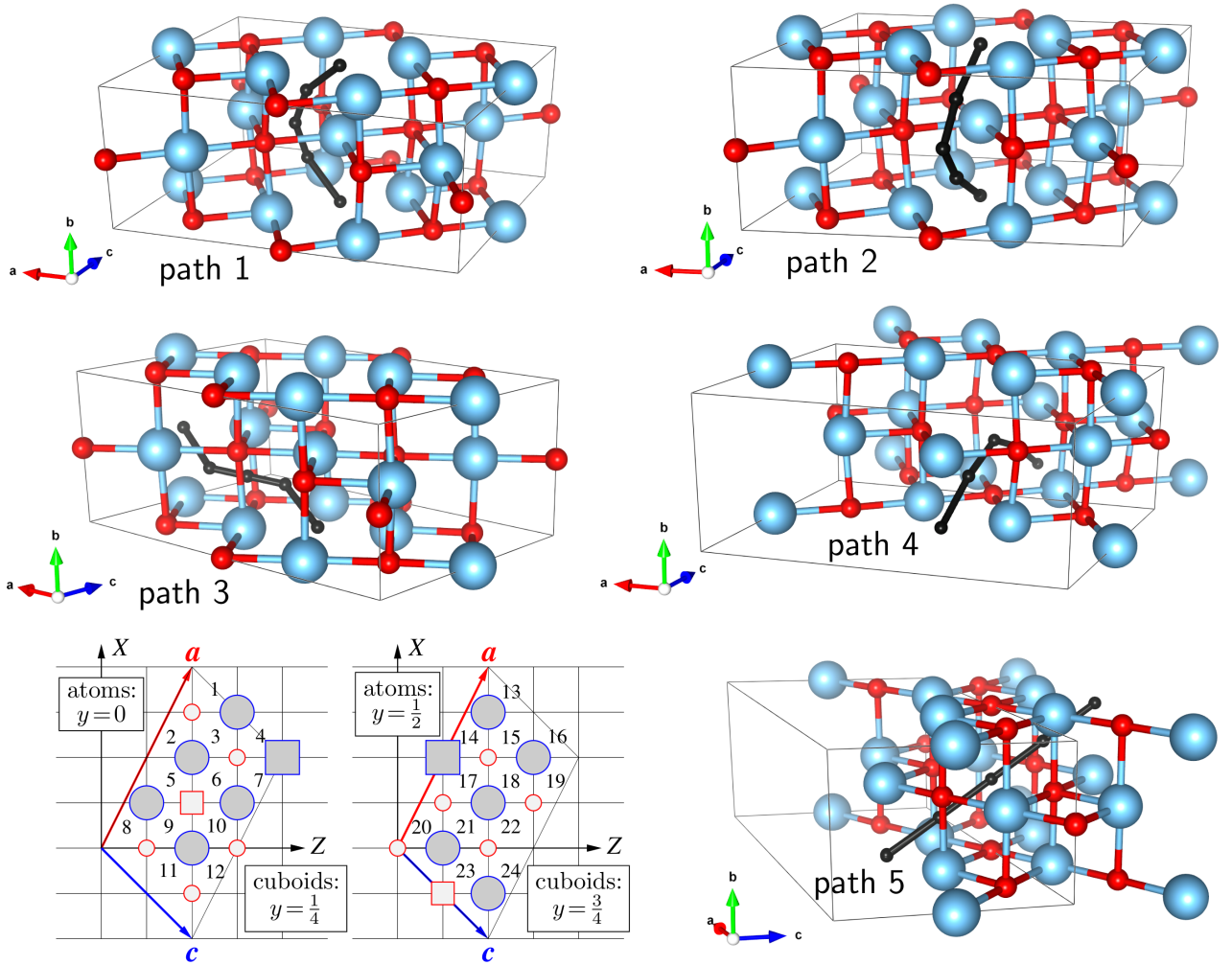


FIG. 1. Crystal structure of monoclinic TiO, in side views (Ti atoms shown large blue and O atoms small red), with five different paths (shown in black color as connected intermediate positions) between adjacent oxygen vacancy sites, and (two panels in the bottom left) as two consecutive (010) planes, with atoms shown as circles and vacancy sites shown as squares. The cuboids (centered $y = \frac{1}{4}$ and $y = \frac{3}{4}$) between consecutive atomic layers are numbered, for reference in the text.

smoothened.

Making reference to numbered cuboids (at the bottom left of Fig. 1) which “pave” two alternating (010) planes of the monoclinic structure, the paths under discussion can be identified as follows.

Both path 1 and path 2 connect the O vacancy sites separated by [010] move, circumventing the Ti atom in between. The path 1 goes (“upwards”, from the O vacancy position with $y=0$) through cuboids 6 and 18 (or, equivalently, 9 and 21); the barrier is obviously anticipated on squeezing through the Ti_2O_2 face in between. The path 2 goes through cuboids 5 and 17 (or, equivalently, 10 and 22). The saddle point at $y = \frac{1}{2}$ occurs now on squeezing through a face which is not complete, because the cuboids in question share a titanium vacancy. Consequently, the path is expected to be pushed either towards or away from this vacancy, and the barrier to become lower than for path 1.

A “watershed” between the paths 1 and 2, with their corresponding saddle points, would be on the Ti–O bond, breaking which is likely to cost much energy.

Path 3 is a $[\frac{1}{2} \frac{1}{2} 0]$ diagonal move, through the cuboids 6 and 3 (or, equivalently, 9 and 11); the bottleneck is squeezing through a complete Ti_2O_2 face underway. Consequently, the barrier is expected to be similar to that on path 1.

Path 4 goes in general [001] direction, making a bow around the O atom situated half-way, through the cuboids 10 and 5 (or, equivalently, through the cuboids 22 and 17 under the $y=0$ plane). This path is likely to go through (or, rather, just close to) the Ti vacancy site (at $y = \frac{1}{2}$) shared by the two cuboids in question. In this sense, the path 4 resembles path 2; the difference is that an oxygen and not titanium atom is circumvented.

Path 5 goes straight along [011] through e.g. the cuboids 10 and 17, via the Ti vacancy site situated half-

way (in the corner shared by the both cuboids). We note in this relation that passing *exactly* through the Ti vacancy on this path is imposed by symmetry (that was not the case of path 2 and 4), therefore the barrier height must match the difference of hydrogen absorption energies in the Ti and the O vacancies. We'll come back to this point in discussing the results below.

In practical calculation of hydrogen absorption energies and diffusion, we were careful to use sufficiently large supercells so that the hydrogen atom could be treated as an isolated impurity, and the effects of spurious periodicity within the hydrogen “sublattice” be minimized.

III. COMPUTATIONAL DETAILS

Electronic total energies and forces (for conjugated-gradient structure relaxation and the extraction of force constants) were calculated within the density functional theory (DFT), using the generalized gradient approximation (GGA) for exchange-correlation functional in the flavor of Perdew–Burke–Ernzerhof (PBE) [34].

Whereas in many calculations done for TiO_2 and Ti_2O_3 , the inclusion of correlation effects beyond the conventional GGA was considered necessary and was treated within “GGA+ U ” scheme or using hybrid functionals (see, e.g., Hu and Metiu[35] for a review), no such need seem to apply to metallic titanium monoxide.

A large part of our calculations have been done with the help of the Quantum ESPRESSO (QE) package [36, 37], using plane waves as basis functions, and otherwise, so that some results would have been cross-checked, with the SIESTA code [38, 39], which relies on atom-centered localized basis functions. The ultrasoft pseudopotentials [40] were employed in QE calculations, whereby Ti $3s$, $3p$, $3d$, $4s$, O $2s$, $2p$ and H $1s$ states were included as valence ones. In SIESTA calculations, norm-conserving pseudopotentials [41] were used, with the attribution of valence states as indicated above, except for the Ti $3s$ states, which were treated as core. The idea of using two methods evolved naturally from a need to apply adequate tools to different tasks, but eventually offered an opportunity to compare parallel predictions as well, which turned out to be helpful in assessment of credibility of numerical results. In fact, even if two codes operate at the same level of theory (DFT/GGA), details of technical implementation may be responsible for slightly different numerical results. Whereas some parameters (\mathbf{k} -mesh, plane-wave cutoffs) can be systematically enhanced to yield necessary precision, the others remain somehow an experience-guided free choice. Such are the generation of pseudopotentials, not identical in two methods, and a construction of basis functions in SIESTA. Whereas QE is robust and free from ambiguity in what regards the choice of bases, SIESTA with its compact yet efficient basis sets might be interesting for trading its applicability to very large systems for an affordable loss in accuracy. In our present compromise, we place on QE our expect-

tations of, a priori, higher accuracy, recognizing at the same time that the size of systems treated with QE risks to be not sufficiently large for making a good model case of isolated impurity. If the methods used are, in a sense, complementary, their combination may help to reasonably estimate the error margin due to inherent technical differences, and to judge about the general credibility of results.

In QE calculations we used $1 \times 2 \times 2$ supercells (40 TiO formula units), and in SIESTA calculations – $1 \times 3 \times 2$ ones (60 TiO formula units), which helped to ensure a more even separation between impurities on the lattice. The \mathbf{k} -mesh used for summations over the Brillouin zone according to the Monkhorst–Pack scheme [42] was more dense in the second case ($6 \times 5 \times 5$ divisions along the reciprocal lattice vectors) than in the first one ($4 \times 4 \times 4$ mesh points). The planewave cutoff for the basis set construction in QE was set to 60 Ry; the cutoff for kinetic energy and charge density expansion to 720 Ry. The `MeshCutoff` parameter for the expansions of residual charge density in SIESTA was set to 300 Ry. The convergence for energy was chosen as 10^{-5} eV between two ionic steps, and the maximum force allowed on each atoms is 0.01 eV/Å. Comparing with earlier works, we can state that our QE calculation setup is closest to that used by Kostenko *et al.* [31] in what regards the code applied, the exchange-correlation potential and the supercell size. The differences are that there was no extrinsic impurities considered in Ref. 31, nor optimization done for lattice parameters (of supercells simulating disorder). Therefore we can address the reader to Fig. 7b of Ref. 31 for inspecting the local densities of states (DOS) in the ordered phase, which exhibit a characteristic pseudogap at the Fermi level, discussed in some of the works cited. Partial DOS in the presence of hydrogen impurity, obtained with SIESTA, will be shown and discussed below. Incorporation energy of a hydrogen atom at a vacancy site is expressed as

$$E_{\text{H}}^I = E_{\text{TiO+H}} - E_{\text{TiO}} - E_{\text{H}}, \quad (1)$$

where $E_{\text{TiO+H}}$ is the total energy of TiO supercell containing a H atom, E_{TiO} is the total energy of pristine TiO supercell, and E_{H} is the energy of isolated H atom. Applying such formula to total energy results obtained with SIESTA (or, with any other method employing atom-centered basis functions) demands to correct for basis set superposition error (BSSE, see Ref. 43). In practical terms of our case, this involved placing hydrogen basis sets (“ghost atoms” not carrying core charges nor electrons) at two relevant (trial) positions for hydrogen adsorption. Either one (for calculating $E_{\text{TiO+H}}$) or none (for E_{TiO}) of these positions were in fact occupied by hydrogen atom, the rest being ghosts. Correspondingly, E_{H} stems from a calculation for the same supercell of the same shape, in which a single (spin-polarized) genuine hydrogen atom cohabits with 121 ghosts.

The inspection of minimum energy paths (MEP) connecting distinct local minima (typically over a saddle point) can be, from the side of theory, conveniently

done by the Nudged Elastic Band (NEB) method, implemented in the QE code. Ref. 44 offers an overview of NEB and other related schemes, which deal with a sequence of intermediate “images”, e.g., conformations of the system subject to interplay of forces “along” and “away from” the path, ensuring the smoothness and the shortness of the latter. In the present calculations, we considered 13 images and (independently) 25 images, in order to check the stability of results against this parameter; `k_min` and `k_max` switches for elastic bands were chosen at 0.2 and 0.3 Ha, respectively.

IV. RESULTS & DISCUSSION

Our calculations included unconstrained structure relaxation of (for reference purposes) pristine monoclinic TiO and, in appropriately enlarged supercell, of hydrogen impurity tentatively placed in various lattice positions. It turned out that the hydrogen remains (the most) stable at oxygen vacancy site, but also at a local energy minimum at titanium vacancy site. Hydrogen escapes from other symmetric positions, e.g., in the centrum of a Ti₂O₂ face, or cutting a Ti–O bond.

A. Equilibrium crystal structures; comparison of methods

Some results reported below (lattice relaxations, energy barriers) have been obtained with two methods, QE and SIESTA. Even if QE, free from ambiguities in constructing the basis functions, might be considered as ultimately more reliable (for the given supercell geometry and similar pseudopotentials), we prefer to expose the SIESTA results along with those by QE. This will help to get some idea of the “credibility margin”, in view of SIESTA being applied to larger-size supercells and yielding some supplementary properties to those explored by QE.

Table I shows the structure parameters of nominal (pristine) TiO, in comparison with experiment, and the (predicted) modification of structure under insertion of hydrogen. SIESTA tends to overestimate the lattice parameters (by at most 2% against the results by Watanabe *et al.*[21]; by $\simeq 5\%$ for the volume) whereas QE seems to perform much better, within 1% of experiment values for every lattice parameter and the volume. However, the dimensions of cages around oxygen vacancies are estimated with SIESTA at least not worse than with QE (judging again by comparison with experiment). What seems important for the following is that the distortion of vacancy cages (measured between two opposite atoms flanking either the vacancy, or the hydrogen atom occupying the vacancy site) upon insertion of hydrogen follows the same pattern according to either QE or SIESTA and seem reliable beyond the calculation “noise”: a roughly uniform expansion (by 1–2%) occurs around hydrogen occupying

the Ti vacancy, whereas around hydrogen at the O vacancy site, an expansion along the long diagonal of the unit cell (i.e., parallel to [10 $\bar{1}$]) is combined with compression in the perpendicular direction ([102]). In Table I, those distances which noticeably (by $\simeq 1\%$) shrink as compared to situation in pristine lattice are overlined in the table; those which expanded (by at least the same margin) are underlined. The average lattice parameters (shown in the three last columns of Table I and the dimensions of the hydrogen-free vacancy cages remain practically unchanged.

B. Adsorption energies, lattice relaxation, electronic structure

Hydrogen incorporation energies calculated according to Eq. (1) yield, with total energies from QE calculations, -2.87 eV at the O vacancy site (hence energetically favorable insertion) and $+0.75$ eV at the Ti vacancy site (hence costing energy). Even if straightforwardly identifiable from the point of view of calculation, these values might be not so easy to relate to experiment, because of ambiguity and difficult reproducibility of reference situations, e.g., molecular hydrogen penetrating the crystal, dissociating, etc. “Straightforward” SIESTA calculations, performed without correcting for BSSE, are in qualitative agreement with QE results, yielding -3.13 eV and $+0.20$ eV for adsorption at the O vacancy and the Ti vacancy sites, respectively. SIESTA calculations staged to minimize the systematic error by excluding the BSSE, e.g., done with the equal number and positions of (either real or ghost) atoms in the three situations relevant for Eq. (1), result in adsorption energies of -2.86 eV (H@□_O) and $+0.73$ eV (H@□_{Ti}). Such good agreement between results of a planewave-basis and a localized-basis methods, even if ideally anticipated, is not always secured technically, and can serve here as an additional argument for the credibility of results.

The variations of total energies have their origin in the fine details of the electronic structure, even if the direct relation might be difficult to trace. Fig. 2 depicts local densities of states at the hydrogen atom at the O vacancy, its nearest Ti neighbors, and both these species averaged over the supercell.

An inspection of Mulliken populations done with the SIESTA code (comparing the fully relaxed situation of a hydrogen insertion with the pristine crystal and ghost atom at the vacancy site) shows an inflow of about 0.1 electrons onto H at the O vacancy site from its surrounding Ti atoms. Interestingly, certain analogy can be found between this system and the rocksalt TiH hydride, addressed in a number of first-principles simulations:[45, 46] the placement of H-related band at $\simeq 6 - 8$ eV below the Fermi level, the charge transfer towards H, the general shape and energy placement of the Ti3d band, the order of magnitude of the formation energy. Especially Smithson *et al.*[46] paid attention to elucidating different

TABLE I. Sizes of empty or H-occupied octahedral cages, according to GGA calculations. For comparison, lattice parameters mapped onto a single monoclinic cell are given. See text for details.

System	dimensions (Ti–Ti in Å) of \square_{O} along...			dimensions (O–O in Å) of \square_{Ti} along...			reduced lattice parameters (Å)*		
	$[10\bar{1}]$	$[102]$	$[010]$	$[10\bar{1}]$	$[102]$	$[010]$	a	b	c
Quantum ESPRESSO calculations ($1 \times 2 \times 2$ supercells)									
pristine	3.905	4.102	4.163	4.247	4.328	4.163	9.319	4.163	5.845
H@ \square_{O}	<u>3.945</u>	4.098	<u>4.110</u>	4.241	4.316	4.162	9.330	4.162	5.839
H@ \square_{Ti}	3.889	4.091	4.171	<u>4.337</u>	<u>4.404</u>	<u>4.309</u>	9.329	4.165	5.853
SIESTA calculations ($1 \times 3 \times 2$ supercells)									
pristine	3.926	4.239	4.226	4.340	4.489	4.247	9.507	4.224	5.954
H@ \square_{O}	<u>3.997</u>	4.242	<u>4.185</u>	4.321	4.479	4.252	9.510	4.229	5.958
H@ \square_{Ti}	3.921	4.241	4.230	<u>4.398</u>	<u>4.535</u>	<u>4.362</u>	9.511	4.224	5.953
X-ray diffraction by Watanabe <i>et al.</i> [†]									
pristine	4.026	4.197	4.142	4.233	4.256	4.142	9.340	4.142	5.855

*Crystallographic angle was within +0.06% in QE calculations and within –0.5% in SIESTA calculations from the experimental value $\beta = 107^\circ 32'$ as reported in [†]Ref. 21; the original attribution of crystallographic parameters is changed in the table to match that in later works.

contributions to the hydride formation energy, including conversion of the metal structure to fcc, expansion to the optimal lattice parameter, and chemical bonding to hydrogen. Under this angle, a H-occupied O vacancy in titanium monoxide is already in “favorable” fcc (rocksalt)-like environment of Ti atoms, whereby the distances between the latter (cf. Ti–Ti size of the O vacancy cage in Table I) roughly matches the lattice parameter of the rocksalt titanium hydride, (4.10 Å, according to Table II of Ref. 46). A discussion around Fig. 6 in the same work specifies the details of charge loss by Ti e_g orbitals in favor of H-centered spherical distribution. Much of this discourse applies to our system as well. Focusing on the details specific for H at the O vacancy in TiO, we note that the Ti DOS is characterized by a dip at the position of the Fermi level, marked in earlier calculations of monoclinic TiO[27, 47]. Among the six Ti atoms neighboring the inserted hydrogen, the two closest to it (compacted towards hydrogen along $[010]$, see Table I) develop the most pronounced difference (two distinct peaks just above the Fermi level, see Fig. 2f) from the pristine (or, lattice-averaged, cf. Fig. 2b) Ti DOS.

The other possible placement of H in TiO, at the Ti vacancy site, is a metastable one, with elevated total energy yet corresponding to a local energy minimum. The peculiarity of this configuration is the local magnetic moment of $1 \mu_B$ inherited from a free hydrogen atom, due to a relative absence of chemical bonding and of charge transfer in either direction between H and its surrounding oxygen atoms. We’ll see in the following that the stability of the magnetic solution is rather sensitive to an off-center displacement of hydrogen. Fig. 3 shows the spatial distribution of the spin density which is strongly localized on the impurity, yet slightly spills out onto the

neighboring O atoms, especially onto those at $\pm \frac{1}{2} \mathbf{b}$. This observation is further reinforced by an inspection of partial DOS concerning H at the Ti site and its neighbors (Fig. 4). The most remarkable feature of the magnetic structure is a narrow majority-spin state just below (by $\simeq 1$ eV) the Fermi level. This state, strongly localized at hydrogen, also manifests itself in the partial DOS of O neighbors, primarily those along $[010]$ – cf. Fig. 4(f). The spatially resolved density of electronic states, integrated in energy just over this peak (done with SIESTA, not shown here) closely reproduces the full spin density revealed by Fig. 3.

Despite the practical absence of the charge transfer, the electronic shells of oxygen atoms are spin polarized to (together over the six atoms) $0.12 \mu_B$. This polarization is two times stronger on the “out-of-plane” atoms [situated at $\pm \frac{1}{2} \mathbf{b}$, marked (f)] in Fig. 4 than on the “in-plane” atoms, marked (d) and (e), as is also revealed by the manifestation of the features below the Fermi energy in the corresponding partial DOS.

For a more systematic insight into the variance of properties at two possible sites for hydrogen, we show in Fig. 5 a simulated smooth transition between them, along the path 5 of Fig. 1. Calculated energy profile, the Mulliken charge at the H atom and the total magnetic moment stem from a row of SIESTA calculations, in which H atom was fixed at the intermediate positions along the path, its nearest neighbors were free to relax, and more distant atoms in the supercell were kept frozen. This can be considered as a forerunner of more general and flexible NEB calculations over the ensemble of paths, to be discussed below. One clearly sees that the relative energy increases along the path, consistently with the energetics discussed above in subsection IV B, until eventually the

magnetic solution sets up, resulting in a modest energy lowering. The “potential well” around the Ti vacancy site is $\approx 1 \text{ \AA}$ wide and $\approx 0.1 \text{ eV}$ (or $\approx 1160 \text{ K}$) deep, so that the zero-point energy for hydrogen in it is about 30 meV , hence this site seems plausible for hypothetical trapping of hydrogen.

One notes that the magnetic solution sets up abruptly and maintains the value of almost exactly $1 \mu_B$, even if the system, being metallic, does not impose an integer value of the magnetic moment. This reinforces the hypothesis that hydrogen at Ti vacancy site behaves as a trapped free atom. Consistently with this view, the Mulliken charge, somehow elevated throughout the “hydride-like” part of the path, drops down to 1.1, a nearly nominal value for a free atom.

The bump in the value of the Mulliken charge at 1/3 of

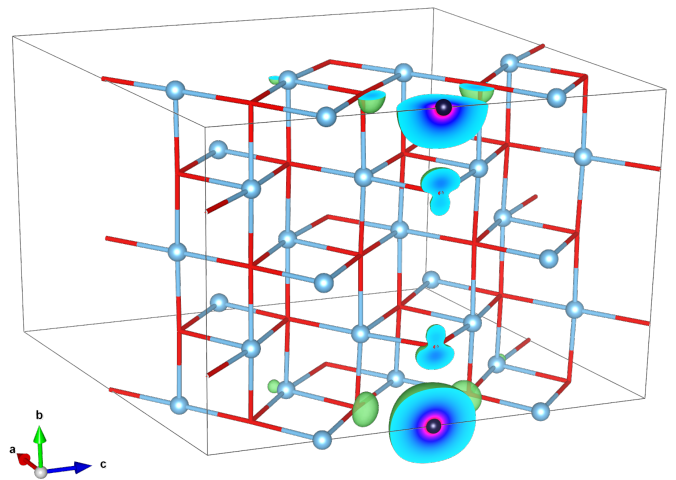


FIG. 3. Spin density map calculated with QE for the supercell with hydrogen (small black sphere) at the Ti vacancy site. Ti atoms are marked by blue spheres; O atoms by red crosses in the wireframe. The isosurface shown in green corresponds to the level of $0.003 \mu_B \text{ \AA}^{-3}$; the color schema in the cuts by the unit cell faces means enhancement from cyan to magenta. As the isosurface increases, the surfaces rapidly become spherical and compact around the H site. In total, there is $1 \mu_B$ per H atom.

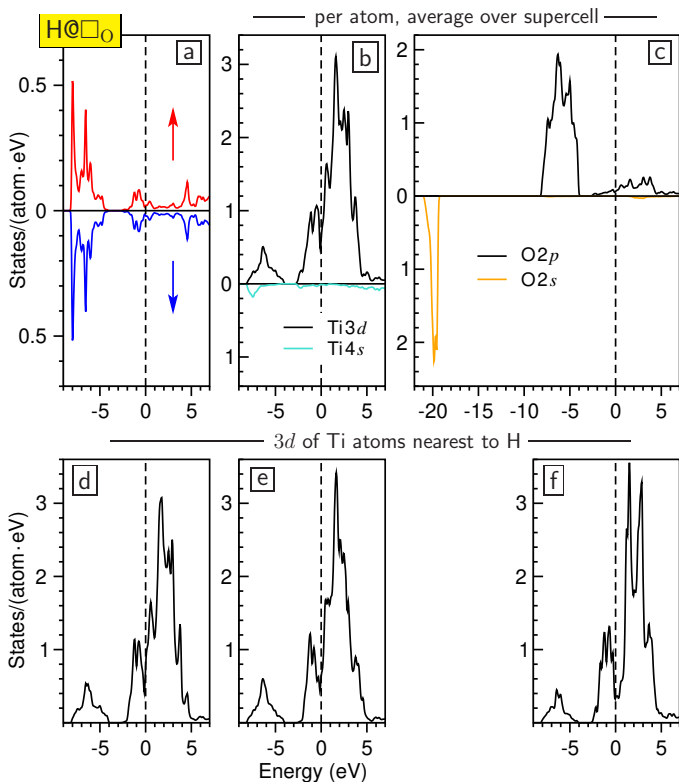


FIG. 2. Partial densities of states (DOS) in relaxed $1 \times 3 \times 2$ (120 atoms) supercell of monoclinic TiO, containing also a hydrogen atom at the oxygen vacancy site, from a SIESTA calculation. Zero energy (dashed vertical line) corresponds to the Fermi energy. The upper row includes (a) spin-resolved DOS of H atom (in fact non-magnetic in this position); (b) $3d$ and $4s$ DOS of Ti (averaged over all Ti sites in the supercell); (c) $2s$ and $2p$ DOS of O (averaged over all O sites in the supercell). The bottom row depicts the $3d$ DOS for three symmetrically distinct pairs of Ti atoms octahedrally bordering the vacancy site occupied by hydrogen, namely (d) atoms situated at $\pm \frac{1}{6}(\mathbf{a} - \mathbf{c})$, (e) – at $\pm \frac{1}{6}(\mathbf{a} + 2\mathbf{c})$, (f) – at $\pm \frac{1}{2}\mathbf{b}$, in units of nominal translation vectors of the monoclinic structure (cf. Fig. 1).

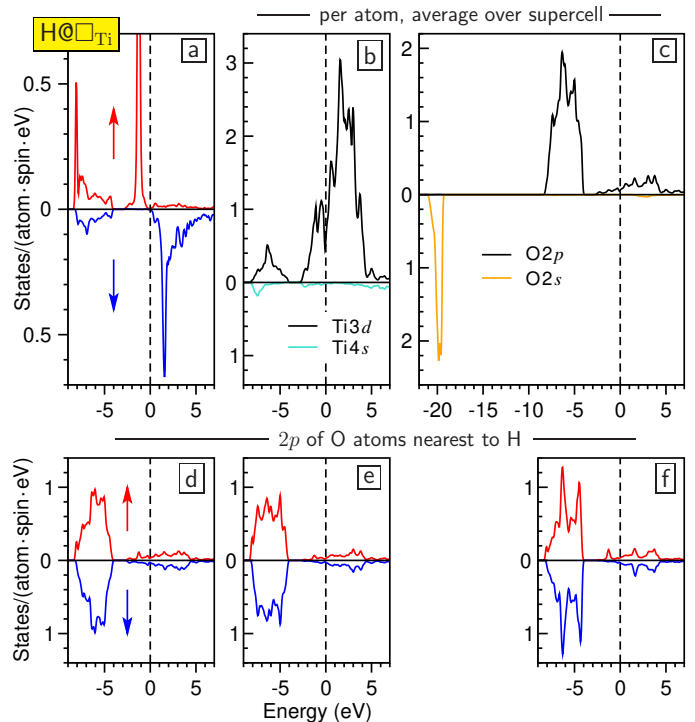


FIG. 4. Similar to Fig. 2, for the case of a hydrogen atom at the titanium vacancy site. The system possesses the magnetic moment of $1 \mu_B$. The bottom row depicts $2p$ DOS of O atoms around the Ti vacancy site, namely (d) atoms situated at $\pm \frac{1}{6}(\mathbf{a} - \mathbf{c})$, (e) – at $\pm \frac{1}{6}(\mathbf{a} + 2\mathbf{c})$, (f) – at $\pm \frac{1}{2}\mathbf{b}$.

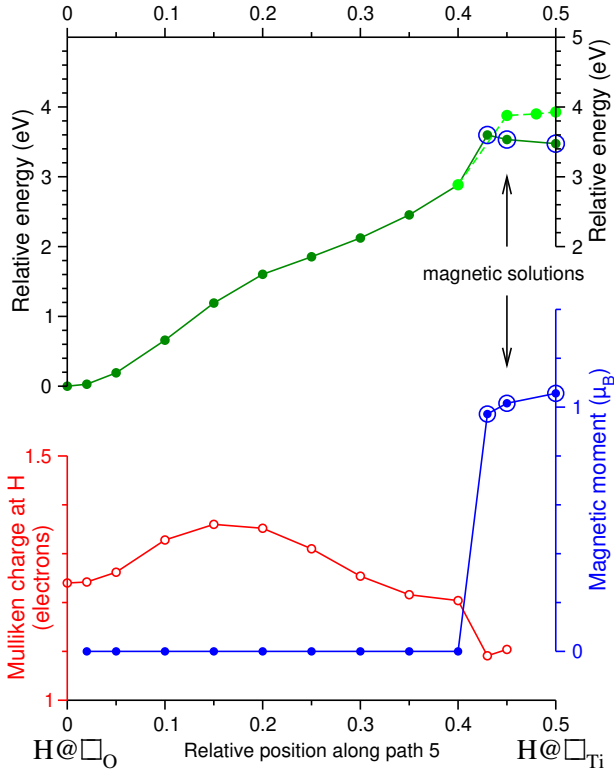


FIG. 5. Variation of total energy, magnetic moment and Mulliken charge at the H atom in the course of the latter’s continuous displacement from O-vacancy to Ti-vacancy position (after SIESTA calculations, allowing the relaxation of atoms along the path). Magnetic solutions, which survive only in small vicinity of the Ti vacancy, are marked by circles. The energy values for their non-magnetic counterparts are indicated by light green dots.

the distance from O-vacancy to Ti-vacancy occurs as the hydrogen atom squeezes between three titanium atoms, across a face of a Ti-octahedron delimiting the O-vacancy cage. This bottleneck is characterised by a charge flow from Ti to H; the total energy curve goes markedly upwards from the direct linear slope. At 2/3 of the distance, the hydrogen atom passes through a triangle of oxygen atoms without a noticeable hybridisation or charge loss, and, being released into the O-octahedron around the Ti vacancy site, it loses extra charge and recovers its free-atom magnetic moment. A slight rearrangement of states within the occupied fraction of $Ti3d-O2p$ bands accounts for a lowering of total energy. Gradually uprising energies of forced zero-spin solutions (cf. light green dots at the right edge of the upper panel in Fig. 5) demonstrate that magnetism of H at the Ti-vacancy site is essential for the (meta)stability of this configuration.

C. Phonons

For additional insight, and also in order to offer some discussion of interesting neutron energy loss spectra published by Skripov *et al.* [20], we calculated the density of vibration modes for H-doped (one atom per supercell) monoclinic TiO. The QE calculation used density functional perturbation method, and SIESTA – frozen phonon calculation. In both these cases, just Γ phonons for the corresponding supercell have been calculated, yielding 243 and 363 modes, respectively. The resulting densities of modes are depicted in Fig. 6, slightly broadened (with halfwidth parameter of 5 cm^{-1}) for better visibility. The abovementioned neutron scattering spectrum is reproduced for comparison, with energy axes properly aligned.

One notes an encouraging agreement between the Ti/O parts of the vibration spectra obtained by two methods,

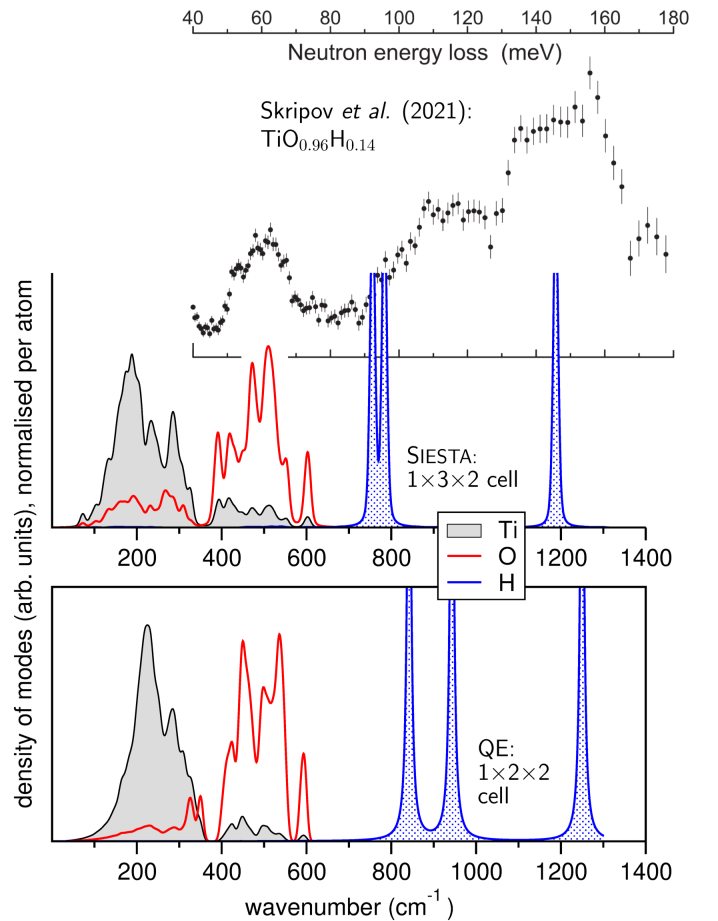


FIG. 6. Densities of vibration modes of TiO with H occupying an oxygen vacancy site (one per supercell indicated), calculated by QE (bottom panel) and SIESTA (middle panel). Neutron scattering spectrum of monoclinic $TiO_{0.96}H_{0.14}$, shown for comparison in the upper panel, is reproduced from Fig. 5 of Ref. 20 – copyright Elsevier (2021). See text for detail.

the degree of such agreement being not a priori obvious in view of certain difference in calculating the electronic structure and the assessment of phonons. As was correctly anticipated in Ref. 20, the low-energy ($\simeq 60$ meV) peak in their neutron scattering spectra (cf. Fig 4 and 5 of the work cited) is due to optical vibrations of oxygen atoms. Moreover, based on inspection of vibration patterns in different modes one can now conclude that the split-off peak at the top of the oxygen vibration band at $\simeq 600$ cm^{-1} , which is also pronounced in the experimental spectrum, reveals the vibrations of 4-coordinated oxygen atoms, i.e., those bordering to Ti vacancies at $\pm \frac{1}{2}\mathbf{b}$.

Hydrogen vibrations make three distinct lines, a close “doublet” at $\simeq 800 - 900$ cm^{-1} and a markedly distant peak at $\simeq 1200$ cm^{-1} . This general picture holds for both SIESTA and QE calculations, even if precise frequencies differ (756, 784, 1188 cm^{-1} in SIESTA calculation vs. 842, 943, 1250 cm^{-1} according to QE). This picture agrees well with the observation by Skripov *et al.*[20] that “... the spectra look like superpositions of two broad bands centered at about 115 meV and about 155 meV”, taking into consideration a “volatility” of calculated frequencies under slightest modification of calculation conditions, due to the smallness of the proton mass. A direct inspection of the modes in question reveals that the vibrations occur along the Ti–Ti axes of the Ti_6 octahedron, i.e., $[102]$, $[010]$ and $[10\bar{1}]$, respectively. The variance in vibration frequencies nicely correlates with the sizes of Ti_6 cages (cf. Table I) and the hence following steepness of the potential well confining the hydrogen vibrations. Namely, the softest of the three vibrations occurs along the direction of the largest Ti–Ti distance, that is $[102]$ according to SIESTA and $[010]$ according to QE. This “contradiction” is not crucial because these two cage dimensions are not much discriminated. On the contrary, the markedly split-off hardest mode represents the vibration along $[10\bar{1}]$, the shortest cage size, in both SIESTA and QE calculations.

Skripov *et al.*[20] suggest that “... the high-energy band at about 155 meV ... may be ascribed to the characteristic environment of H in the monoclinic phase”, to which statement we now offer an adjusting explanation.

It was emphasized in Ref. 20 that “... the volume of the voids formed by oxygen vacancies is too large for H atoms, so that a hydrogen atom can be easily displaced from the geometrical center of the vacancy” and “...for a considerable number of H atoms, the nearest-neighbor environment is no longer octahedral”. In fact we show that off-center displacement is not crucial for explaining broad peaks and that, even when preserving an octahedral environment, slightest modifications of the latter’s shape and size due to all possible distant imperfections in the lattice are capable to generate a broad band of hydrogen vibration frequencies, typical for a spectra of real materials.

D. Dissociation of H_2 molecule

In the study of hydrogen uptake and diffusion in metals, it is generally accepted that the H_2 molecule is first physisorbed at the surface and may then overcome the activation barrier for dissociation (see, e.g., a discussion around Fig. 1 of Kirchheim and Pundt [48]). Hydrogen atoms may further be chemisorbed and eventually diffuse into the material. As in the discussion about hydrogen diffusion (see next subsection), quantum effects may be important in overcoming the activation barrier; an early representative work to this effect, simulating dissociative adsorption (of H_2 on Cu surface), was done by Mills and Jónsson [49]. We do not address this issue here in details, but, as the geometry and the properties of TiO are somehow different from common metals, we wonder whether a hydrogen molecule may fit into, and survive intact within, the oxygen vacancy cage.

As it turns out in the course of conjugate-gradient total energy minimization (see Fig. 7, one example out of several trial ones starting from different initial orientations), the molecule eventually “almost dissociates”, doubling the nominal H–H bond length to $\simeq 1.4$ Å. It looks like every hydrogen atom preferentially “couples” to three closest Ti atoms, in the spirit of the remark made in the previous subsection about the oxygen vacancy cage being too large for a hydrogen atom. We did not manage to reproduce a definite dissociation, when one of the H atoms would flee the Ti_6 cage delimiting an oxygen vacancy site, because this would require an energy inflow to overcome a barrier (see next subsection); however, such event seems to be within grasp for a molecular dynamical high-temperature simulation. Indeed, an energy step of $\simeq 1.2$ eV (see Fig. 7) separates the “weakened”/expanded H_2 molecule from a situation when one of its constituent

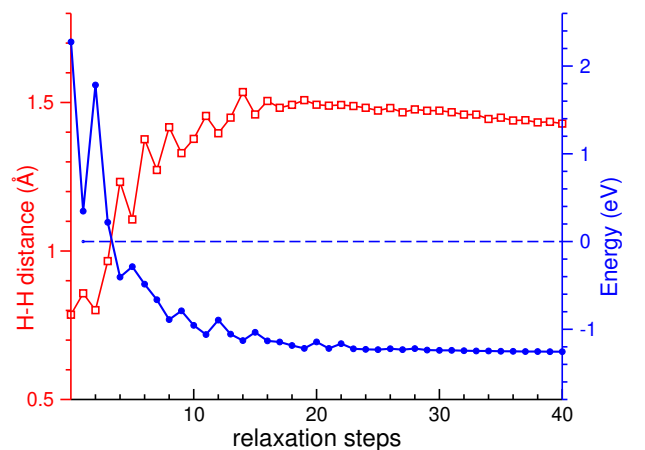


FIG. 7. Evolution of interatomic distance (left scale, red squares) and total energy (right scale, blue dots) of an H_2 molecule placed in an oxygen vacancy, after a SIESTA calculation. Zero energy corresponds to a situation with a single H atom relaxed at oxygen vacancy site and another one being free. See text for details.

H atoms is promoted out of the crystal. An irrevocable dissociation and diffusion away from the original site of an atom remaining within the crystal may presumably cost less energy.

E. Energy barriers for hydrogen atom hopping over oxygen vacancy sites

We turn now to the discussion of scenarios, outlined earlier in Section II, of how a hydrogen atom, initially trapped in oxygen vacancy site, can be brought onto an adjacent similar site. Practical calculations have been done according to NEB formalism implemented in QE code; comparison of results obtained with 13 and with 25 images along the path gives us credibility in what regards the barrier height, whereby the barrier profile obtained with 25 images is more smooth and permits to discuss some details. All the paths must in principle be left-right symmetric; this is not exactly the case for paths 4 and 5, due to numerical “noise” in the course of practical NEB calculations. From the end points, the energy profile departs nicely parabolically, which is not so obvious with 13 images but much better represented for 25-images path (cf. bottom right panel in Fig. 8). Assuming that the hydrogen atom vibrates *alone* around its equilibrium position at the extremity of each path, the corresponding frequency from fitting the corresponding force constant falls between 776 cm^{-1} (along the path 4 or 5) to 816 cm^{-1} (along the path 3). This nicely matches the prediction from the “full” phonon calculation addressed above.

We turn now to a discussion of different paths. The paths 4 and 5 seem degenerate; that follows indeed from an observation that the mid-point in each of them is the same, – namely, a Ti vacancy site, from which the path can equally turn “downwards” or “upwards”, consistently to drawings in the two last panels of Fig. 1. One sees a shallow local minimum on top of the barrier, already mentioned in subsection IV B as a manifestation of magnetic solution. Therefore, this is a metastable position for a hydrogen atom, rather than a genuine saddle point. However, there is a subtlety. If the mid-point of path 5 is placed at the Ti vacancy site by the crystal symmetry, the mid-point of path 4 is subject to technical “drift”, depending on the spring constant along the NEB, or other details of the algorithm used. As a result, the path may tend to get shortened by displacing its midpoint slightly “downwards” (closer to the oxygen atom, as is suggested by a drawing of path 4 in Fig. 1), correspondingly climbing the midpoint energy upwards. Such a “perturbation” would eventually destroy the local minimum on top of the barrier. This was not the case in our calculation which preserved the similarity of the energy profiles along path 4 and path 5. We note that the barrier height in corresponding NEB calculations, 3.71 eV , is expectedly close to the difference between previously discussed adsorption energies at the Ti vacancy and the O vacancy sites, i.e.,

$+0.75 - (-2.87) = 3.62 \text{ eV}$. The mismatch of 0.09 eV may be attributed to the technical difference between the constraints imposed in the course of “conventional” conjugate-gradient search and in a NEB calculation. We emphasize that the profile of path 5 is an “improved version” of the energy profile preliminarily scanned in a row of SIESTA calculations and depicted in Fig. 5.

The “bottleneck” of the paths 1 and 3 is the hydrogen atom squeezing through the intact Ti–O–Ti–O square face. The difference is that on the “upward” (see Fig. 1) path 1 this face is within a (010) lattice plane, whereas for path 3 it makes a (20 $\bar{1}$) plane. In path 2, the hydrogen atom passes through an incomplete square face, missing a Ti atom at one of its corners. The snapshots of the atomic relaxation within the corresponding planes is shown in Fig. 9, in comparison with the unperturbed (no hydrogen) situation. One notes that, on passing through the “bottleneck”, the hydrogen atom only slightly repels its Ti neighbors (Ti–Ti diagonal increases by $\sim 3\%$) but quite considerably ($\sim 27\%$ of the initial distance) pushes apart the O neighbors. This repulsion can be understood from purely electrostatic arguments, since hydrogen, like oxygen, is more electronegative than titanium and receives some electron density from the latter. For this reason, skirting an oxygen atom in the mid-point of path 4 does not bring this path considerably to the side (downwards in Fig. 1), as discussed above, whereas the path 2, laid in fact across a cavity with missing Ti atom, comes quite close to the remaining Ti atom, which the path skirts.

With the “bottlenecks” on path 1 and path 3 being so similar (cf. Fig. 9), we cannot suggest any obvious reason for the difference in corresponding barrier heights other than the “natural” anisotropy of the crystal structure. In any case, the path 2 undoubtedly possesses the lowest energy barrier, since it does not include a passage between closely placed two Ti and two O atoms, pushing those latter to the sides. Consequently, the path 2 is expected to dominate among hypothetical channels of hydrogen diffusion, to which the other paths, possessing the barrier energy of the same order of magnitude, should contribute in parallel without being a priori excluded.

The height of the barrier measured from the endpoint minima, i.e. the activation energy E_a , may in principle serve to estimate the reaction (e.g., diffusion) rate D via the Arrhenius equation (see, e.g., the review by Gomer [50] for detail):

$$D = \nu \exp\left(-\frac{E_a}{k_B T}\right). \quad (2)$$

A more detailed analysis of different contributions to the flux of hydrogen atoms induced by gradient of concentrations and involving hoppings over the barriers was given by Kirchheim and Pundt [48], culminating in Eq. (55) of their work. The frequency prefactor ν (called “attempt frequency” in Ref. 48) may vary in very broad ranges, depending on the reaction type; estimations for proton diffusion in TiO might be not obvious. Zhdanov [51]

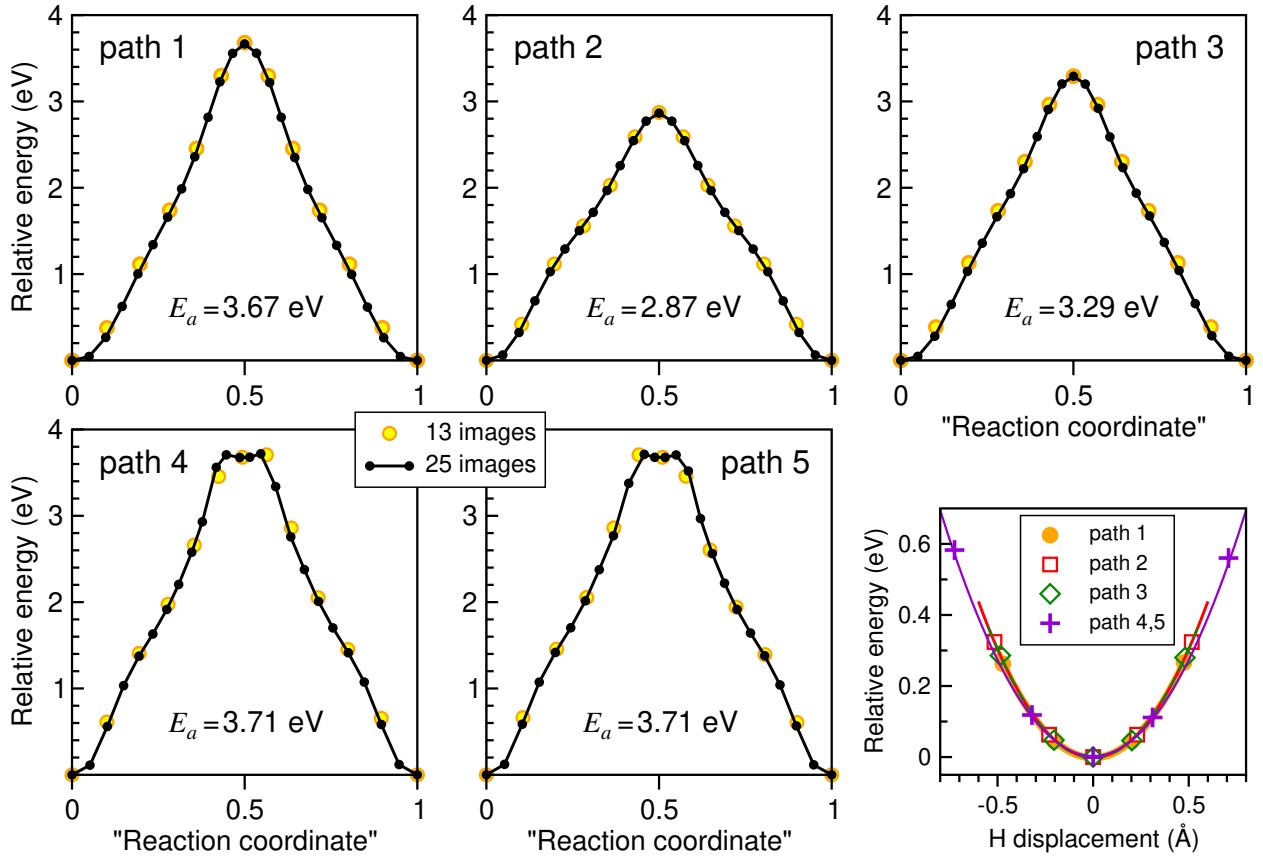


FIG. 8. NEB energy profiles for H atom displacement along the five paths specified in Fig. 1. Results of calculations performed with 13 and with 25 images along each path are shown for comparison. The barrier height is indicated for each path. In the bottom right panel, the total energy is traced as function of absolute displacement of the hydrogen atom from equilibrium position, near the beginning and the end of each path.

summarized a number of parameters from the literature in Tables 1 and 2 of his review work; for instance, for desorption of H_2 from Pt ν makes 10^6 s^{-1} and from other different metal surfaces – 10^{12} to 10^{17} s^{-1} . In any case,

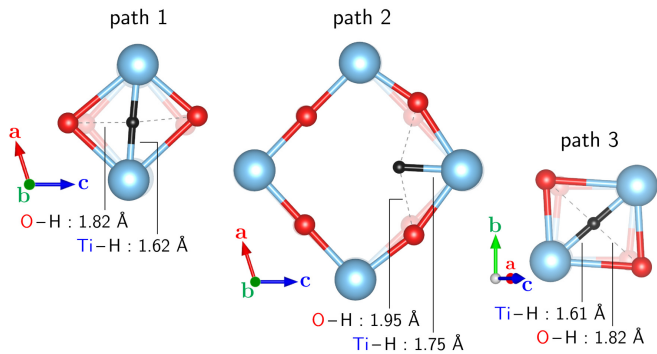


FIG. 9. Optimized structures at the saddle points of paths 1, 2, and 3. Distances between the hydrogen atom and its nearest Ti and O neighbors are indicated. The corresponding equilibrium structures in the absence of hydrogen are shown faded in the background.

huge heights of the barriers relative to the ambient thermal energy ($k_B T = 26 \text{ meV}$ at 25°C) in practical sense identifies the diffusion over barriers as an utterly improbable event. A general understanding is that quantum tunneling plays an important role in hydrogen transport in metals [52, 53]. A more detailed analysis along this line would go beyond the scope of the present work, but it is likely to be responsible for much higher mobility of hydrogen in different materials than it could be understood in terms of hopping over the barriers. Coming back specifically to TiO, Skripov *et al.* [20] set $\sim 10^5 \text{ s}^{-1}$ as the upper limit on the hydrogen jump rate in strongly substoichiometric and nearly stoichiometric H-doped TiO, referring to the NMR line width: “...H atoms in titanium monoxides appear to be immobile on the NMR frequency scale up to 370 K”. As an explanation, Skripov *et al.* evoke spatial separation between the oxygen vacancy sites. We reinforce this conclusion by identifying barrier heights as unusually high, by the standards of hydrogen diffusion in metals. For comparison, Pozzo et Alfé [54] calculated the diffusion barriers for hydrogen atoms over the Mg(0001) surface doped with different transition metals to span the values from nearly zero (Ag doping) to – the largest

among the systems probed – 0.94 eV (Zr doping) and 0.75 eV (Ti doping).

In view of high barriers separating the hydrogen adsorption sites, and in agreement with the experimental evidence so far available, TiO seems to be promising for accumulating hydrogen, even if not so in terms of easiness of the hydrogen diffusion. This can give rise to interesting applications, with a perspective of extension over other related materials. Interestingly, the group of Lefort *et al.* reported [55, 56] an enormous capacity to accommodate hydrogen (up to 2.9 wt.%) for highly substoichiometric titanium carbide, $\text{TiC}_{0.6}$, which was not the case in weakly substoichiometric $\text{TiC}_{0.9}$. The authors attribute this property to the presence of long-range-ordered carbon vacancies in $\text{TiC}_{0.6}$, in contrast to $\text{TiC}_{0.9}$. In view of the similarity of the crystal structures of titanium carbide and monoxide, this discovery is stimulating for the extension of our present study.

V. CONCLUSIONS

Summarizing, we performed first-principles calculations of electronic structure, lattice vibrations and possible diffusion barriers in monoclinic TiO doped with H atom. Our results reinforce the earlier available experimental evidence that hydrogen atoms enter the oxygen vacancy sites, the related energy gain now being estimated as $\simeq 2.87$ eV. Moreover, the Ti vacancy sites were identified as possible metastable positions for adsorbed hydrogen atoms, unfavorable in energy (with respect to the case of desorbed hydrogen) by 0.75 eV. The Ti vacancy site makes a mid-point of two possible diffusion paths (those with the highest barrier, 3.71 eV) connecting two adjacent O vacancy sites. The lowest-energy path (with the barrier height of 2.87 eV) goes around a Ti atom at a distance of 1.75 Å from it. Different paths involve squeezing the H atom through different crystal structure bottlenecks, whereby the O atoms are considerably pushed away and the Ti atoms are somehow attracted towards the hydrogen atom. The estimated values of barrier height are too high to account for an appreciable hydrogen diffusion rate, assuming the hoppings

over barriers as the principal diffusion mechanism. It seems plausible that quantum tunneling processes may play an important role, as is the case with hydrogen diffusion in other materials. Calculations of lattice vibration spectrum are consistent with earlier reported results of inelastic neutron diffusion; the remaining deviations offer a substance for discussion about the placement of hydrogen atoms within the oxygen-vacancy cages.

Under an angle of possible applications, our study demonstrates that (and explains why) the Ti monoxide may absorb considerable amount of hydrogen, which however tends to remain immobile in the sense of diffusivity through the lattice. This might be promising, e.g., for superconductivity, the tendency for which can be addressed in a separate study. As another prospective extension towards practical needs, the uptake and dissociation of molecular hydrogen at the surface, an issue almost routinely simulated with some other materials, may seem interesting here. In the context of fundamental science, the manifestation of quantum effects in the uptake and diffusion of hydrogen may deserve a thorough study; moreover, an interplay of vacancy ordering and diffusion may happen to be interesting. In any case, an enrichment of experimental evidence will be highly motivating.

ACKNOWLEDGMENTS

The authors thank Dr. Alexander Skripov for careful reading of the manuscript and for useful comments. The authors thank Elsevier for granting a permission to reproduce Fig. 5 from the article “Hydrogen in nonstoichiometric cubic titanium monoxides: X-ray and neutron diffraction, neutron vibrational spectroscopy and NMR studies” by A.V. Skripov *et al.*, originally published in Journal of Alloys and Compounds (Copyright Elsevier 2021) Vol. **887**, 161353. S.V.H. and M.R.M. acknowledge a partial financial support by the Research Council of the University of Tehran. S.V.H. and A.P. thank the mesocenter of calculation EXPLOR at the Université de Lorraine (project 2019CPMXX0918) for granting access to computational resources.

-
- [1] J. O. Abe, A. P. I. Popoola, E. Ajenifuja, and O. M. Popoola, Hydrogen energy, economy and storage: Review and recommendation, *International Journal of Hydrogen Energy* **44**, 15072 (2019).
 - [2] J. B. Goodenough, Perspective on engineering transition-metal oxides, *Chemistry of Materials* **26**, 820 (2014).
 - [3] Y. Sun, T. Zhang, C. Li, K. Xu, and Y. Li, Compositional engineering of sulfides, phosphides, carbides, nitrides, oxides, and hydroxides for water splitting, *J. Mater. Chem. A* **8**, 13415 (2020).
 - [4] Y. Zhu, Q. Lin, Y. Zhong, H. A. Tahini, Z. Shao, and H. Wang, Metal oxide-based materials as an emerging family of hydrogen evolution electrocatalysts, *Energy Environ. Sci.* **13**, 3361 (2020).
 - [5] J. Song, C. Wei, Z.-F. Huang, C. Liu, L. Zeng, X. Wang, and Z. J. Xu, A review on fundamentals for designing oxygen evolution electrocatalysts, *Chem. Soc. Rev.* **49**, 2196 (2020).
 - [6] X. Shang, J.-H. Tang, B. Dong, and Y. Sun, Recent advances of nonprecious and bifunctional electrocatalysts for overall water splitting, *Sustainable Energy & Fuels* **4**, 3211 (2020).
 - [7] M. S. Burke, L. J. Enman, A. S. Batchellor, S. Zou, and S. W. Boettcher, Oxygen evolution reaction electro-

- catalysis on transition metal oxides and (oxy)hydroxides: Activity trends and design principles, *Chemistry of Materials* **27**, 7549 (2015).
- [8] S. Wu, K.-Y. Tseng, R. Kato, T.-S. Wu, A. Large, Y.-K. Peng, W. Xiang, H. Fang, J. Mo, I. Wilkinson, Y.-L. Soo, G. Held, K. Suenaga, T. Li, H.-Y. T. Chen, and S. C. E. Tsang, Rapid interchangeable hydrogen, hydride, and proton species at the interface of transition metal atom on oxide surface, *Journal of the American Chemical Society* **143**, 9105 (2021).
- [9] H. Yoon, Y. Kim, E. J. Crumlin, D. Lee, K. Ihm, and J. Son, Direct probing of oxygen loss from the surface lattice of correlated oxides during hydrogen spillover, *The Journal of Physical Chemistry Letters* **10**, 7285 (2019).
- [10] M. S. Whittingham, Hydrogen motion in oxides: from insulators to bronzes, *Solid State Ionics* **168**, 255 (2004), proceedings of the Workshop on Hydrogen: Ionic, Atomic and Molecular Motion.
- [11] H. Nolan and M. P. Browne, Hydrogen energy currency: Beyond state-of-the-art transition metal oxides for oxygen electrocatalysis, *Current Opinion in Electrochemistry* **21**, 55 (2020).
- [12] W. Oelerich, T. Klassen, and R. Bormann, Metal oxides as catalysts for improved hydrogen sorption in nanocrystalline Mg-based materials, *Journal of Alloys and Compounds* **315**, 237 (2001).
- [13] W. Oelerich, T. Klassen, and R. Bormann, Hydrogen sorption of nanocrystalline Mg at reduced temperatures by metal-oxide catalysts, *Advanced Engineering Materials* **3**, 487 (2001).
- [14] X.-L. Yin, M. Calatayud, H. Qiu, Y. Wang, A. Birkner, C. Minot, and C. Wöll, Diffusion versus desorption: Complex behavior of H atoms on an oxide surface, *ChemPhysChem* **9**, 253 (2008).
- [15] H. Feng, Z. Xu, L. Ren, C. Liu, J. Zhuang, Z. Hu, X. Xu, J. Chen, J. Wang, W. Hao, Y. Du, and S. X. Dou, Activating titania for efficient electrocatalysis by vacancy engineering, *ACS Catalysis* **8**, 4288 (2018).
- [16] K. Zhu, F. Shi, X. Zhu, and W. Yang, The roles of oxygen vacancies in electrocatalytic oxygen evolution reaction, *Nano Energy* **73**, 104761 (2020).
- [17] X. Hu, M. Trudeau, and D. M. Antonelli, Hydrogen storage in microporous titanium oxides reduced by early transition metal organometallic sandwich compounds, *Chemistry of Materials* **19**, 1388 (2007).
- [18] Y. Li, Z. G. Yu, L. Wang, Y. Weng, C. S. Tang, X. Yin, K. Han, H. Wu, X. Yu, L. M. Wong, D. Wan, X. R. Wang, J. Chai, Y.-W. Zhang, S. Wang, J. Wang, A. T. S. Wee, M. B. H. Breese, S. J. Pennycook, T. Venkatesan, S. Dong, J. M. Xue, and J. Chen, Electronic-reconstruction-enhanced hydrogen evolution catalysis in oxide polymorphs, *Nature Communications* **10**, 3149 (2019).
- [19] J. Swaminathan, R. Subbiah, and V. Singaram, Defect-rich metallic titania ($\text{TiO}_{1.23}$) – an efficient hydrogen evolution catalyst for electrochemical water splitting, *ACS Catalysis* **6**, 2222 (2016).
- [20] A. V. Skripov, A. V. Soloninin, A. A. Valeeva, A. I. Gusev, A. A. Rempel, H. Wu, and T. J. Udovic, Hydrogen in nonstoichiometric cubic titanium monoxides: X-ray and neutron diffraction, neutron vibrational spectroscopy and NMR studies, *Journal of Alloys and Compounds* **887**, 161353 (2021).
- [21] D. Watanabe, J. R. Castles, A. Jostsons, and A. S. Malin, The ordered structure of TiO, *Acta Crystallographica* **23**, 307 (1967).
- [22] S. P. Denker, Relation of bonding and electronic band structure to the creation of lattice vacancies in tiox, *Journal of Physics and Chemistry of Solids* **25**, 1397 (1964).
- [23] A. A. Valeeva, A. A. Rempel, M. A. Müller, K. J. Reichle, G. Tang, W. Sprengel, and H.-E. Schaefer, Identification of atomic vacancies in titanium monoxide by electron microdiffraction and positron annihilation, *physica status solidi (b)* **224**, R1 (2001).
- [24] M. D. Banus, T. B. Reed, and A. J. Strauss, Electrical and magnetic properties of TiO and VO, *Phys. Rev. B* **5**, 2775 (1972).
- [25] A. Gusev, Niobium monoxide superstructures, *JETP Letters* **111**, 176 (2020).
- [26] A. Neckel, P. Rastl, R. Eibler, P. Weinberger, and K. Schwarz, Results of self-consistent band-structure calculations for ScN, ScO, TiC, TiN, TiO, VC, VN and VO, *Journal of Physics C: Solid State Physics* **9**, 579 (1975).
- [27] C. Leung, M. Weinert, P. B. Allen, and R. M. Wentzcovitch, First-principles study of titanium oxides, *Phys. Rev. B* **54**, 7857 (1996).
- [28] D. A. Andersson, P. A. Korzhavyi, and B. Johansson, Thermodynamics of structural vacancies in titanium monoxide from first-principles calculations, *Phys. Rev. B* **71**, 144101 (2005).
- [29] J. M. Schoen and S. P. Denker, Band structure, physical properties, and stability of TiO by the augmented-plane-wave virtual-crystal approximation, *Phys. Rev.* **184**, 864 (1969).
- [30] J. Graciani, A. Márquez, and J. F. Sanz, Role of vacancies in the structural stability of α -TiO: A first-principles study based on density-functional calculations, *Phys. Rev. B* **72**, 054117 (2005).
- [31] M. G. Kostenko, A. V. Lukoyanov, V. P. Zhukov, and A. A. Rempel, Vacancies in ordered and disordered titanium monoxide: Mechanism of b1 structure stabilization, *Journal of Solid State Chemistry* **204**, 146 (2013).
- [32] S. Kajita, T. Minato, H. S. Kato, M. Kawai, and T. Nakayama, First-principles calculations of hydrogen diffusion on rutile $\text{TiO}_2(110)$ surfaces, *The Journal of Chemical Physics* **127**, 104709 (2007).
- [33] D. Watanabe, J. R. Castles, A. Jostsons, and A. S. Malin, Ordered structure of titanium oxide, *Nature* **210**, 934 (1966).
- [34] J. P. Perdew, K. Burke, and M. Ernzerhof, Generalized gradient approximation made simple, *Phys. Rev. Lett.* **77**, 3865 (1996).
- [35] Z. Hu and H. Metiu, Choice of U for DFT+ U calculations for titanium oxides, *The Journal of Chemical Physics* **115**, 5841 (2011).
- [36] P. Giannozzi, S. Baroni, N. Bonini, M. Calandra, R. Car, C. Cavazzoni, D. Ceresoli, G. L. Chiarotti, M. Cococcioni, I. Dabo, A. Dal Corso, S. de Gironcoli, S. Fabris, G. Fratesi, R. Gebauer, U. Gerstmann, C. Gougoussis, A. Kokalj, M. Lazzeri, L. Martin-Samos, N. Marzari, F. Mauri, R. Mazzarello, S. Paolini, A. Pasquarello, L. Paulatto, C. Sbraccia, S. Scandolo, G. Sclauzero, A. P. Seitsonen, A. Smogunov, P. Umari, and R. M. Wentzcovitch, Quantum ESPRESSO: a modular and open-source software project for quantum simulations of materials, *Journal of Physics: Condensed Matter* **21**, 395502 (2009).
- [37] P. Giannozzi, O. Andreussi, T. Brumme, O. Bunau, M. Buongiorno Nardelli, M. Calandra, R. Car, C. Cavaz-

- zoni, D. Ceresoli, M. Cococcioni, N. Colonna, I. Carnimeo, A. Dal Corso, S. de Gironcoli, P. Delugas, R. A. DiStasio Jr, A. Ferretti, A. Floris, G. Fratesi, G. Fugallo, R. Gebauer, U. Gerstmann, F. Giustino, T. Gorni, J. Jia, M. Kawamura, H.-Y. Ko, A. Kokalj, E. Küçükbenli, M. Lazzeri, M. Marsili, N. Marzari, F. Mauri, N. L. Nguyen, H.-V. Nguyen, A. Otero-de-la Roza, L. Paulatto, S. Poncé, D. Rocca, R. Sabatini, B. Santra, M. Schlipf, A. P. Seitsonen, A. Smogunov, I. Timrov, T. Thonhauser, P. Umari, N. Vast, X. Wu, and S. Baroni, Advanced capabilities for materials modelling with Quantum ESPRESSO, *Journal of Physics: Condensed Matter* **29**, 465901 (2017).
- [38] J. M. Soler, E. Artacho, J. D. Gale, A. García, J. Junquera, P. Ordejón, and D. Sánchez-Portal, The SIESTA method for *ab initio* order- N materials simulation, *Journal of Physics: Condensed Matter* **14**, 2745 (2002).
- [39] A. García, N. Papior, A. Akhtar, E. Artacho, V. Blum, E. Bosoni, P. Brandimarte, M. Brandbyge, J. I. Cerdá, F. Corsetti, R. Cuadrado, V. Dikan, J. Ferrer, J. Gale, P. García-Fernández, V. M. García-Suárez, S. Garcí, G. Huhs, S. Illera, R. Korytár, P. Koval, I. Lebedeva, L. Lin, P. López-Tarifa, S. G. Mayo, S. Mohr, P. Ordejón, A. Postnikov, Y. Pouillon, M. Pruneda, R. Robles, D. Sánchez-Portal, J. M. Soler, R. Ullah, V. W.-z. Yu, and J. Junquera, Siesta: Recent developments and applications, *The Journal of Chemical Physics* **152**, 204108 (2020).
- [40] D. Vanderbilt, Soft self-consistent pseudopotentials in a generalized eigenvalue formalism, *Phys. Rev. B* **41**, 7892 (1990).
- [41] N. Troullier and J. L. Martins, Efficient pseudopotentials for plane-wave calculations, *Phys. Rev. B* **43**, 1993 (1991).
- [42] H. J. Monkhorst and J. D. Pack, Special points for Brillouin-zone integrations, *Phys. Rev. B* **13**, 5188 (1976).
- [43] F. B. van Duijneveldt, J. G. C. M. van Duijneveldt-van de Rijdt, and J. H. van Lenthe, State of the art in counterpoise theory, *Chemical Reviews* **94**, 1873 (1994).
- [44] D. Sheppard, R. Terrell, and G. Henkelman, Optimization methods for finding minimum energy paths, *The Journal of Chemical Physics* **128**, 134106 (2008).
- [45] A. Fujimori and N. Tsuda, Electronic structure of non-stoichiometric titanium hydride, *Journal of the Less Common Metals* **88**, 269 (1982).
- [46] H. Smithson, C. A. Marianetti, D. Morgan, A. Van der Ven, A. Predith, and G. Ceder, First-principles study of the stability and electronic structure of metal hydrides, *Phys. Rev. B* **66**, 144107 (2002).
- [47] S. R. Barman and D. D. Sarma, Electronic structure of TiO_x ($0.8 < x < 1.3$) with disordered and ordered vacancies, *Phys. Rev. B* **49**, 16141 (1994).
- [48] R. Kirchheim and A. Pundt, 25 - hydrogen in metals, in *Physical Metallurgy (Fifth Edition)*, edited by D. E. Laughlin and K. Hono (Elsevier, Oxford, 2014) fifth edition ed., pp. 2597–2705.
- [49] G. Mills and H. Jónsson, Quantum and thermal effects in H_2 dissociative adsorption: Evaluation of free energy barriers in multidimensional quantum systems, *Phys. Rev. Lett.* **72**, 1124 (1994).
- [50] R. Gomer, Diffusion of adsorbates on metal surfaces, *Reports on Progress in Physics* **53**, 917 (1990).
- [51] V. P. Zhdanov, Arrhenius parameters for rate processes on solid surfaces, *Surface Science Reports* **12**, 185 (1991).
- [52] H. K. Birnbaum and C. P. Flynn, Hydrogen tunneling states in niobium, *Phys. Rev. Lett.* **37**, 25 (1976).
- [53] K. W. Kehr, Theory of the diffusion of hydrogen in metals, in *Hydrogen in Metals I: Basic Properties*, edited by G. Alefeld and J. Völkl (Springer Berlin Heidelberg, Berlin, Heidelberg, 1978) pp. 197–226.
- [54] M. Pozzo and D. Alfè, Hydrogen dissociation and diffusion on transition metal (=Ti, Zr, V, Fe, Ru, Co, Rh, Ni, Pd, Cu, Ag)-doped Mg(0001) surfaces, *International Journal of Hydrogen Energy* **34**, 1922 (2009).
- [55] A. Gringoz, N. Glandut, and S. Valette, Electrochemical hydrogen storage in $\text{TiC}_{0.6}$, not in $\text{TiC}_{0.9}$, *Electrochemistry Communications* **11**, 2044 (2009).
- [56] J. Nguyen, N. Glandut, C. Jaoul, and P. Lefort, Hydrogen insertion in substoichiometric titanium carbide, *International Journal of Hydrogen Energy* **40**, 8562 (2015).